Atmos. Chem. Phys., 15, 9399–9412, 2015
www.atmos-chem-phys.net/15/9399/2015/
doi:10.5194/acp-15-9399-2015

Atmospheric Chemistry and Physics
Open Access

NO_x emission estimates during the 2014 Youth Olympic Games in Nanjing

J. Ding[1,2], R. J. van der A[1], B. Mijling[1], P. F. Levelt[1,2], and N. Hao[3]

[1]Royal Netherlands Meteorological Institute (KNMI), De Bilt, the Netherlands
[2]Delft University of Technology, Delft, the Netherlands
[3]German Aerospace Center (DLR), Oberpfaffenhofen, Germany

Correspondence to: J. Ding (jieying.ding@knmi.nl)

Received: 12 February 2015 – Published in Atmos. Chem. Phys. Discuss.: 4 March 2015
Revised: 31 July 2015 – Accepted: 12 August 2015 – Published: 24 August 2015

Abstract. The Nanjing Government applied temporary environmental regulations to guarantee good air quality during the Youth Olympic Games (YOG) in 2014. We study the effect of those regulations by applying the emission estimate algorithm DECSO (Daily Emission estimates Constrained by Satellite Observations) to measurements of the Ozone Monitoring Instrument (OMI). We improved DECSO by updating the chemical transport model CHIMERE from v2006 to v2013 and by adding an Observation minus Forecast (OmF) criterion to filter outlying satellite retrievals due to high aerosol concentrations. The comparison of model results with both ground and satellite observations indicates that CHIMERE v2013 is better performing than CHIMERE v2006. After filtering the satellite observations with high aerosol loads that were leading to large OmF values, unrealistic jumps in the emission estimates are removed. Despite the cloudy conditions during the YOG we could still see a decrease of tropospheric NO_2 column concentrations of about 32 % in the OMI observations when compared to the average NO_2 columns from 2005 to 2012. The results of the improved DECSO algorithm for NO_x emissions show a reduction of at least 25 % during the YOG period and afterwards. This indicates that air quality regulations taken by the local government have an effect in reducing NO_x emissions. The algorithm is also able to detect an emission reduction of 10 % during the Chinese Spring Festival. This study demonstrates the capacity of the DECSO algorithm to capture the change of NO_x emissions on a monthly scale. We also show that the observed NO_2 columns and the derived emissions show different patterns that provide complimentary information. For example, the Nanjing smog episode in December 2013 led to a strong increase in NO_2 concentrations without an increase in NO_x emissions. Furthermore, DECSO gives us important information on the non-trivial seasonal relation between NO_x emissions and NO_2 concentrations on a local scale.

1 Introduction

Reducing air pollution is one of the biggest environmental challenges currently in China. Nearly 75 % of urban areas are regularly polluted in a way that was considered unsuitable for their inhabitants in 2004 (Shao et al., 2006). In mega cities and their immediate vicinities, air pollutants exceed the Chinese Grade-II standard (80 $\mu g\,m^{-3}$ for daily NO_2) on 10–30 % of the days between 1999 to 2005 (Chan and Yao, 2008). Air pollution is directly related to the economic growth in China and its accompanying increase of energy consumption. In the last 2 decades, air pollutants persistently increased in China. For instance, satellite measurements showed that NO_2 column concentrations increased by about 50 % from 1996 to 2005 (Irie, 2005; Richter et al., 2005; van der A et al., 2006). By combining satellite observations with air quality models, Itahashi et al. (2014) showed that the strong increase of NO_2 columns over East China was caused by a doubling of NO_x ($NO_x = NO + NO_2$) emissions from 2000 to 2010. Zhang et al. (2007) found that NO_x emissions increased by 70 % between 1995 and 2006 and Lamsal et al. (2011) found that anthropogenic NO_x emissions increased 18.8 % during the period 2006 to 2009.

Nanjing, the capital of Jiangsu Province, is a highly urbanized and industrialized city located in East China, in

Table 1. Air-quality regulations taken by the Nanjing authorities in the year of YOG2014. The period is the start time of different regulations. The italic regulations are still effective after the YOG.

Period	Regulations
1 May–30 June	The local government started to shut down the coal-burning factories.
1–15 July	All coal-burning factories have been shut down.
16–31 July	The work on one third of construction sites was stopped. The parking fees in downtown increased sevenfold.
1–15 August	The work on 2000 construction sites was stopped. Heavy-industry factories reduced manufacturing by 20 percent. *Vehicles with high emissions were banned from the city*. Open space barbecue restaurants were closed. *900 electric buses and 500 taxis have been put into operation.*
16–31 August	The work at all construction sites was put on hold.

the northwest part of the Yangtze River Delta (YRD). By 2012, the area of Nanjing had a population of 8.2 million (Nanjing statistical Bureau, 2013). The YRD is one of the largest economic and most polluted regions in China. Tu et al. (2007) found that the largest fraction of air pollution by NO_x and SO_2 can be attributed to local sources in Nanjing. Li et al. (2011) concluded that air pollutant concentrations and visibility demanded urgent air pollution regulations in the YRD region. From 16 to 29 August 2014, the Youth Olympic Games (YOG) were held in Nanjing. To guarantee good air quality during the Games, the city government carried out temporary strict environmental regulations with 35 directives from May to August. Other cities in the YRD cooperated with Nanjing to ensure good air quality during the Games. The periods with the main regulations are shown in Table 1. In addition, several technical improvements have been implemented to reduce pollution from heavy industry and power plants.

For previous major international events in China, local authorities have tried to comply with the air quality standards of the World Health Organization (WHO), which has a limit of $200\,\mu g\,m^{-3}$ for hourly NO_2 concentrations. For each event, the local government imposed restrictions on heavy industry, construction and traffic. In 2008 the Beijing Municipal Government implemented a series of air pollution control measures for Beijing and surrounding cities to guarantee good air quality for the 29th Olympic Games. These control measures significantly reduced the emissions and concentrations of pollutants. Satellite data show that the NO_2 column concentrations decreased at least 40 % compared to previous years (Mijling et al., 2009; Witte et al., 2009). Both bottom-up and top-down emission estimates show a decrease of about 40 % in NO_x emissions (Wang et al., 2009; Mijling et al., 2013; Wang et al., 2010). During the 2010 World Expo in Shanghai the NO_2 column was reduced by 8 % from May to August according to an analysis of Hao et al. (2011) of space-based measurements compared to previous years. In November 2010 emission reduction measures introduced by the Guangzhou authorities also successfully improved air quality for the Asian Games. Wu et al. (2013) claimed a NO_x emission reduction of 43.5 % based on mobile DOAS measurements. The emission reduction of NO_x based on model simulations was estimated to be about 40 % (Liu et al., 2013).

However, to study the effectiveness of the air quality measures, it is not enough to look at the concentration measurements alone, as the reduction of air pollutants can also be affected by favorable meteorological conditions. Emissions need to be derived to better show the effect of temporary air quality regulations carried out for the Games. Up-to-date emission data are difficult to obtain, as most emission inventories are developed by a bottom-up approach based on statistics on source sector, land-use and sector-specific emission factors.

The bottom-up approach introduces large uncertainties in the emission inventories. To improve emission inventories, a top-down approach can be used by estimating emissions from satellite observations (Streets et al., 2013). For constraining emissions of short-lived species, Martin et al. (2003) used the ratio of the simulated to the observed column to scale a priori emissions. They used optimal estimation to weigh the a priori emission inventory with the top-down estimates, resulting in an a posteriori inventory with error estimates. This method assumes that the relationship between emissions and concentrations is not affected by transport. Non-linear and non-local relations between emission and concentration can be indirectly solved by applying the method iteratively (e.g. Zhao and Wang, 2009), although a posteriori error estimates are lost in this way. Kurokawa et al. (2009) and Stavrakou et al. (2008) used 4DVAR techniques to estimate emissions by applying an adjoint model of the chemistry transport model to calculate the sensitivities. Another popular data assimilation method is the ensemble Kalman filter (Evensen, 2003), which does not require an adjoint model and is relatively easy to implement. As an extension of the Kalman filter, it employs a Monte Carlo approach to represent the uncertainty of the model system with a large stochastic ensemble. Whenever the filter requires statistics such as mean and covariance, these are obtained from the sample statistics of the ensemble (Miyazaki et al., 2012).

To get fast updates for short-lived air pollutants, Mijling and van der A (2012) designed a Daily Emission estimates Constrained by Satellite Observation (DECSO) algorithm. DECSO is an inversion method based on an extended Kalman filter. The algorithm only needs one forward model run of a chemical transport model (CTM) to calculate all local and non-local emission/concentration relations. It updates emissions by addition instead of scaling, enabling the detection of unaccounted emission sources.

In this study, we use the latest version of DECSO with OMI satellite data to study how the environmental regulations affect the NO_x emissions in Nanjing during the 2014 YOG. Detecting emission changes for Nanjing is challenging, as it is a smaller city than, e.g., Beijing. In addition, Nanjing is in one of the most populated areas of China close to Shanghai with a population of about 24 million. Therefore we have introduced a few improvements in the DECSO algorithm to better resolve small-scale emission changes in time and location. The improvements consist of an updated CTM and better filtering of erroneous satellite observations. The emission estimates will be based on the satellite observations of OMI, taking advantage of its high spatial resolution needed to resolve the changes in the Nanjing area. With this improved algorithm we will compare the NO_x emissions during the YOG with NO_x emissions of the previous year in the Yangtze Delta River.

2 Methods

2.1 Emission estimates

For the emission estimates of NO_x over China we use the DECSO algorithm (Mijling and van der A, 2012). It uses a CTM to simulate the NO_2 concentrations and daily satellite observations of NO_2 column concentrations to constrain NO_x emissions. The algorithm is based on an extended Kalman filter to get new emission estimates by optimizing NO_2 column concentrations of model and satellite observations. The inclusion of sensitivities of NO_2 column concentrations on the NO_x emissions in other locations is an essential part of DECSO. A terrain-following trajectory analysis is used in this calculation to describe the transport of NO_2 over the model domain for a time interval between two overpasses of the satellite instrument. This approach results in a fast algorithm suitable for daily estimates of NO_x emissions on a $0.25° \times 0.25°$ resolution. A detailed description of DECSO v1 can be found in Mijling and van der A (2012).

The CTM used in DECSO is CHIMERE (Schmidt, 2001; Bessagnet et al., 2004; Menut et al., 2013). CHIMERE is implemented on a $0.25° \times 0.25°$ spatial grid over East Asia from 18 to 50° N and 102 to 132° E. It contains eight atmospheric layers up to 500 hPa. The meteorological input for CHIMERE is the operational meteorological forecast of the European Centre for Medium-Range Weather Forecasts (ECMWF) with a horizontal resolution of approximately $25 \times 25\,km^2$. The Multi-resolution Emission Inventory for China (MEIC) (He, 2012) for 2010 gridded to a resolution of $0.25° \times 0.25°$, is used for the initial emissions in DECSO. Outside China, where no MEIC emissions are defined, the emission inventory of INTEX-B (Q. Zhang et al., 2009) is used. As the emission sector definition used in MEIC and INTEX-B does not match the 11 activity sectors according to the SNAP (Selected Nomenclature for Air Pollution) 97, which are internally used in the CHIMERE model, we estimate the redistribution of the emissions over the sectors (see Table 2).

As mentioned by Mijling and van der A (2012), to compare CHIMERE simulations with satellite observations, we extend the modeled vertical profiles from 500 hPa to the tropopause by adding a climatological partial column, which is from an average of a 2003–2008 run of the global chemistry transport model TM5. The simulated NO_2 column concentrations on the model grid are redistributed to the satellite footprints. To enable direct comparison between simulated and observed tropospheric vertical column, the averaging kernel from the satellite retrieval is then applied to the modeled vertical profile.

In this study, we used an updated version of DECSO, which is referred to as DECSO v3a. In particular, the calculation speed has been improved in this update. DECSO does not distinguish between biogenic emissions and the anthropogenic sectorial emissions. Emission differences are attributed to anthropogenic contribution only, i.e., the biogenic emissions are assumed to be modeled correctly by the CTM. Emission updates are distributed by ratio over the sectors (power, industry, transport, domestic) as described by the a priori emission inventory. If a grid cell is dominated by power plant emissions, however, emission updates are attributed to the power sector only. The locations of power plants are provided to the algorithm as additional a priori information. In DECSO v3a, the emission injection height has been made sector-dependent. Emissions are injected in the lowest three model layers of the CTM; each sector having its own characteristic vertical emission distribution. For example, transport emissions are released at the surface, while power plant emissions are fully released in the third model layer corresponding to a typical smokestack height. Trajectory calculations of the observed species are crucial in the determination of the source-receptor relations. The DECSO algorithm uses meteorological wind fields (the same as used in the CTM) to calculate how the content of a tropospheric column is advected over the model domain. Here, the injection heights is distributed according to the modeled vertical NO_x distribution. In DECSO, the forward trajectory calculation is changed to a backward trajectory calculation, i.e., the source-receptor relations are calculated backward in time, based on the height distribution of NO_x modeled at satellite overpass time.

In DECSO v3a, tuned synthetic error estimates E_{obs} estimates are used, derived from the original satellite observation

Table 2. Estimated redistribution of MEIC sectors over SNAP 97 sectors.

MEIC sectors SNAP 97 sectors	Power	Industry	Transport	Residential	Agriculture
Combustion in energy and transformation industries	1	–	–	–	–
Non-industrial combustion plants	–	–	–	1	–
Combustion in manufacturing industry	–	0.3	–	–	–
Production process	–	0.3	–	–	–
Extraction and distribution of fossil fuels and geothermal energy	–	0.4	–	–	–
Solvent and other product use	–	–	–	–	–
Road transport	–	–	1	–	–
Other mobile sources and machinery	–	–	–	–	–
Waste treatment and disposal	–	–	–	–	–
Agriculture	–	–	–	–	1
Other source and sinks	–	–	–	–	–

via

$$E_{\text{obs}} = f \cdot E_{\text{sat}} + (1 - f) \cdot (0.5 \cdot E_{\text{sat}}), \quad \text{with } f = e^{(-\frac{c_{\text{sat}}}{2})}, \tag{1}$$

where E_{sat} is the original observation error from the retrieval method and C_{sat} is the retrieved NO_2 column of the satellite observation. The unit in this formula is 10^{15} molecules cm^{-2}. The modified errors give more weight to satellite observations with high values during the assimilation by reducing their relative error while maintaining the dominating absolute error for low values (typically around 0.5×10^{15} molecules cm^{-2}). In this way, DECSO better captures new emission points or high-emission episodes.

2.2 Satellite observations

In this study, satellite observations from the Dutch-Finnish Ozone Monitoring Instrument (OMI) on NASA's Aura satellite (Levelt et al., 2006) are used in DECSO. The satellite was launched on 15 July 2004 into a sun-synchronous polar orbit at 705 km altitude. OMI is a nadir-viewing spectrometer measuring the atmosphere-backscattered solar light in the ultraviolet-visible (UV/VIS) range from 270 to 500 nm with a spectral resolution of about 0.5 nm. The 114° wide view of OMI results in a swath width of 2600 km, providing daily global coverage in about 14 orbits. The local overpass time is around 13:30 local time (LT). The pixel size of OMI is $24 \times 13\,\text{km}^2$ at nadir and increases to about $150 \times 28\,\text{km}^2$ at the end of the swath.

We use the tropospheric NO_2 vertical column concentrations retrieved with the Dutch OMI NO_2 retrieval (DOMINO) algorithm version 2 (Boersma et al., 2011). The data set is available on the Tropospheric Emissions Monitoring Internet Service (TEMIS) portal (http://www.temis.nl). The DOMINO algorithm first obtains NO_2 slant columns from the OMI reflectance spectra by using Differential Optical Absorption Spectroscopy (DOAS). After separating the stratospheric and tropospheric contribution to the slant column, DOMINO converts the tropospheric slant column to a vertical column with the tropospheric air mass factor (AMF) (Boersma et al., 2007, 2011). DOMINO v2.0 mainly improves the NO_2 air mass factor by improved radiative transfer, surface albedo, terrain height, clouds and a priori vertical NO_2 profiles. The bias between DOMINO v2.0 and Multi-Axis Differential Optical Absorption Spectroscopy (MAX-DOAS) ground observations at five locations is only -10 ± 14 % over China and Japan (Irie et al., 2012). The DOMINO algorithm does not explicitly account for the effect of aerosols on the solar radiation. Rather it is indirectly accounted for by the higher cloud fraction in aerosol contaminated scenes. However, Lin et al. (2014) concluded that especially in China the effects of aerosols and surface reflectance anisotropy have implications for retrievals of NO_2 from OMI and suggested that exclusion of high aerosol scenes supports better emission estimates at fine spatial and temporal scales.

Since 25 June 2007, OMI data have been affected by the so-called row anomaly, which deteriorates the spectral observations for particular viewing directions of OMI (Boersma et al., 2011; Kroon et al., 2011). Twenty-nine out of the 60 rows are affected by the row anomalies and no longer used after 1 January 2011. We also filter out the four pixels at either side of the swath because the size of these pixels is 3 times larger than the model grid cell. After the filtering, the largest footprint is about $75 \times 21\,\text{km}^2$. To reduce the influence of cloudy and bright surface scenes on the quality of the retrieval product, we use only observations having a surface albedo lower than 20 % to remove observations over snow and ice (Product Specification Document of DOMINO v2 on www.temis.nl). The observations with clouds below 800 hPa are also filtered out as these retrievals are very sensitive to small differences in the NO_2 profile shape and the retrieved cloud height. Mijling and van der A (2012) filter out the observations with a cloud fraction higher than 20 %. Based on this filtering, there are no tropospheric NO_2 satellite observations over Nanjing during the YOG due to the cloudy conditions at the overpass time of the satellite. Thus, to obtain more NO_2 satellite observations, we use observations with a

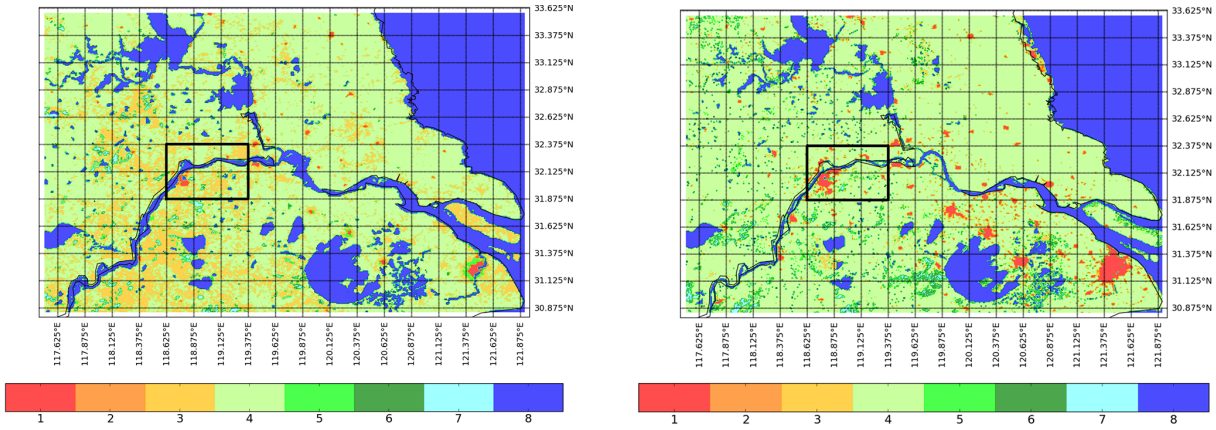

Figure 1. Land use over the Jiangsu Province from Global Land Cover Facility (1994) (left) and the GlobCover Land Cover (2009) (right) and as used in CHIMERE v2006 and CHIMERE v2013. The eight categories are: 1. Urban, 2. Barren land, 3. Grassland, 4. Agricultural land, 5. Shrubs, 6. Needleleaf forest, 7. Broadleaf forest, 8. Water. The solid rectangle (about $50 \times 90\,\mathrm{km}^2$) indicates the 6 grid cells that cover the Nanjing area.

cloud radiance fraction lower than 70 % (comparable with a cloud fraction of about 30–35 %) instead of the cloud fraction lower than 20 %. From our analysis of the satellite data we conclude that as a result of this new limit on the cloud fraction the error on the measurements increases by less than 20 % and without introducing biases. Yet this effect is compensated by the advantage that more data become available. The number of observations over the whole domain increases by about 37 % on average.

2.3 Ground-based observations

To validate the model results in Nanjing, we use available independent measurements from the national in situ observation network, which are collected and maintained by the China National Environmental Monitoring Center (CNEMC). The aqicn.org team publishes the hourly Air Quality Index (AQI) of specific air pollutants, such as NO_2, SO_2, and particulate matter (PM_{10} and $PM_{2.5}$), on their website based on the measurements from CNEMC. The AQI is calculated by the conversion table from the Technical Regulation on Ambient Air Quality Index in China published by the Ministry of Environmental Protection (http://kjs.mep.gov.cn/hjbhbz/bzwb/dqhjbh/jcgfffbz/201203/W020120410332725219541.pdf). We use the same table to convert the AQI back to the surface concentration unit of $\mu g\,m^{-3}$. For this study, the NO_2 hourly in situ measurements of Nanjing for the period of April 2013 to December 2014 are used. The location of these measurements is the Nanjing People's Government building, which is located in the center of Nanjing. Interpretation of the validation results is troubled by the absence of peripheral information of the in situ measurements. For instance, the type of instrument is unknown and the exact location of the measurement such as the height or the distance to a local traffic road is unclear.

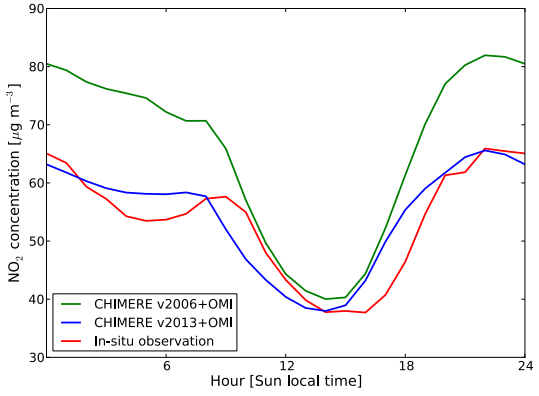

Figure 2. The diurnal cycle in Nanjing from January to August 2014 according to in situ observations, OMI-assimilated CHIMERE v2013 and CHIMERE v2006.

3 Improvements of DECSO

3.1 Model improvement

The performance of the CTM is important for the DECSO results. CHIMERE v2006 is an outdated model version which has been used in DECSO algorithm versions up to v3a. To improve the emission estimation results, we updated the CTM to CHIMERE v2013 (DECSO v3b).

The new model adds biogenic emissions of six species: isoprene, α-ioporene, α-pinene, β-pinene, limonene, ocimene and NO. These biogenic emissions are calculated by the model preprocessor using the MEGAN model and land use data (Menut et al., 2013). The added biogenic emissions can affect the emissions estimated for rural areas as biogenic NO emissions in rural areas cannot be neglected in summertime. Compared to the old version of CHIMERE,

the new model version includes a more advanced scheme for secondary organic aerosol chemistry. In addition, the chemical reaction rates are updated and a new transport scheme is used in the new CHIMERE model. The new CHIMERE model includes the emission injection height profile for different emission sectors. For CHIMERE v2013 we use the same input data except for the land use data. We use land use data from the GlobCover Land Cover (GCLC version 2.3) database, which are updated for the year 2009, while the land use database included in CHIMERE v2006 is the Global Land Cover Facility (GLFC) giving the land use of 1994. As China is a fast developing country, the land use may have large differences in 15 years due to urbanization (see Fig. 1). Thus, the updated land use database will positively affect the model simulations over China.

To assess the effect of the new CTM, we run DECSO v3a and DECSO v3b for the period January 2013 to August 2014. Figure 2 shows the comparison of the average diurnal cycle of surface NO_2 concentrations from the two CHIMERE models with in situ observations in Nanjing averaged for January to August 2014. We select the $0.25° \times 0.25°$ model grid cell that contains the in situ measurement location. According to GCLC database, 70 % of the grid cell is urban area. We see that the surface NO_2 concentration of CHIMERE v2013 during nighttime is closer to the observations than for CHIMERE v2006. Our earlier model evaluations of CHIMERE showed that the nocturnal surface NO_2 concentrations simulated by CHIMERE v2006 are usually too high in urban areas caused by unrealistically low boundary layer heights and too little vertical diffusion. In CHIMERE v2013, the boundary layer heights over urban areas are limited by a minimum boundary layer height. As expected, v2013 improves the surface concentration simulation at nighttime, while differences during daytime are rather small compared to the in situ observations. We calculate the bias and root mean square error (RMSE) between the model results and in situ observations. The bias of CHIMERE v2013 is 3.7 $\mu g\,m^{-3}$, which is 10 $\mu g\,m^{-3}$ smaller than for CHIMERE v2006. The difference of RMSE between the two models is very small: the RMSE of CHIMERE v2013 is 28 $\mu g\,m^{-3}$ and of CHIMERE v2006 is 31 $\mu g\,m^{-3}$. For the satellite overpass time, the bias improves from 4.4 to 1.8 $\mu g\,m^{-3}$ while the RMSE remains the same. However, in urban areas the local sources have transient influences on in situ observations. Blond et al. (2007) concluded that urban in situ observations of NO_2 cannot be used for the validation of a CTM model with low spatial resolution because the representativeness of the in situ measurement for the grid cell is very low. In spite of this, by using the 8-month average of the diurnal cycle to reduce the transient influences on the in situ measurements, we see some improvements for averaged NO_2 concentrations in CHIMERE v2013.

In order to get a more comprehensive validation of the model results, we compare the two CHIMERE models with OMI satellite observations. During the data assimilation of

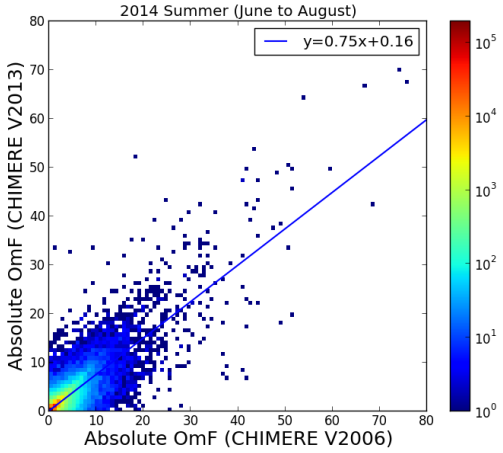

Figure 3. The comparison of the absolute OmF (10^{15} molecules cm^{-2}) of CHIMERE v2006 and CHIMERE v2013 for the whole East Asian domain from June to August. The colorbar represents the frequency of satellite observations for that specific value of OmF.

DECSO the daily Observation minus Forecasts (OmF) values have been stored. The OmF is a common measure for the forecasting capabilities of the model in the data assimilation. We compare the absolute OmF of both models for the summer (June to August) of 2014 in Fig. 3. In the Figure a linear regression is fitted through the data points that shows the absolute OmF of CHIMERE v2013 is lower than that of CHIMERE v2006 indicating a better performance of CHIMERE v2013 in summertime. However, the absolute OmF of two models is similar in wintertime. Since biogenic emissions are negligible in wintertime, this may point to an effect of the missing biogenic emissions in the older version of CHIMERE. Based on these comparisons we selected CHIMERE v2013 in DECSO v3b for NO_x emission estimates in this study.

3.2 Quality control of satellite data

Earlier studies showed that the DOMINO v2 retrievals do not account enough for the effect of high aerosol concentrations on NO_2 columns (see Sect. 2.2) and at the same time we know that high aerosol concentrations are a significant problem in most megacities in China. When checking the time series of NO_x emissions over Nanjing for 2013 by DECSO v3b, we find some suspicious fluctuations at particular days. At these dates the derived NO_x emissions drop to zero in 1 day and then slowly increase again to the previous emission levels in the following days. These unrealistic emission updates concurred with extreme OmF values (lower than -5×10^{15} or higher than 10×10^{15} molecules cm^{-2}) with relative small OmF variances, which are calculated as the quadratic sum of model and observation errors (Fig. 4). In the time period of our study there are 20 days with these extreme OmF values, 6 are positive and 14 are negative. All

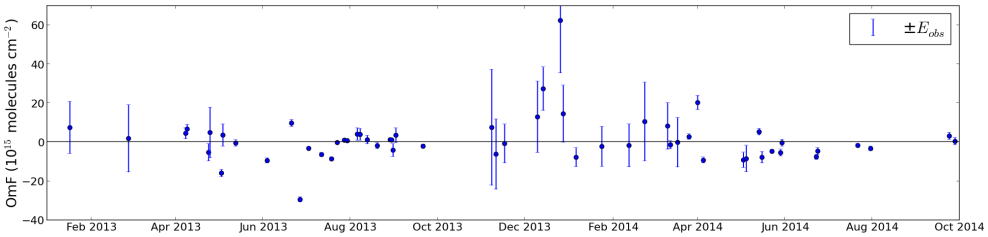

Figure 4. The time series of the OmF from January 2013 to September 2014 for the single grid cell over the center of Nanjing. The error bar is the root mean square error of observations (E_{obs}).

are having a significant impact on the NO_x emissions. For most of those 20 days, the in situ observations of PM_{10} from CNEMC (see Sect. 2.3) show high aerosol concentrations, which are above 100 µg m^{-3} in Nanjing. We also see a strong haze above Nanjing for all these 20 days from visual inspection of the MODIS RGB images. In addition, we noticed that the MODIS images showed higher cloud fractions than the fractions retrieved from OMI observations. The deviating of cloud fraction information from the OMI satellite retrieval is probably due to the aerosol conditions, which are not taken into account in the cloud retrieval algorithm (Acarreta et al., 2004; Stammes et al., 2008). High aerosol concentrations can not only complexly affect the cloud fraction and cloud pressure retrieval but also directly affect the NO_2 retrieval and results in either over- or under- estimated NO_2 column concentrations (Lin et al., 2014).

Figure 5 shows an example of such an extreme case for East China on 6 May 2013 with high (positive) OmF values in combination with low observational uncertainties (Eq. 1). In the image we identify two areas with satellite observations that are at least 10×10^{15} molecules cm^{-2} higher than the model forecast. One is over the Hulunbuir sand land at the border of China and Mongolia, the other one is around the Bohai Bay. We compared the observations with the MODIS RGB and Aerosol Optical Depth (AOD) images on that day (Fig. 6). The MODIS AOD image shows high aerosol values around the Bohai Bay and over the Hulunbuir sand land. The RGB image of MODIS shows haze around the Bohai Bay, which indicates that high aerosol concentrations are presented in that area. However, the aerosol information is not used in the retrieval of the DOMINO NO_2 product leading to NO_2 observations that are strongly deviating from the model forecast.

The effect of high aerosol concentrations on the NO_2 retrieval is non-linear and depends strongly on both the type of aerosol and its concentration. Also the height of the aerosol layer and the presence of clouds play a role (Leitão et al., 2010; Lin et al., 2014). It is therefore difficult to filter out outliers in the observed NO_2 based on aerosol data. In the data assimilation it is assumed that the OmF distribution is Gaussian and the OmF can be used to filter outliers from the data. So far, no OmF outlier criterion has been used in DECSO. Our previous analysis, however, shows the need for the detection of outliers. A filter has to be implemented with care, to avoid the algorithm becoming insensitive to new emission sources such as new power plants. Not losing sensitivity to new emission sources is also the reason we do not choose a relative filter criterion. We select an OmF filter criterion in the range of $[-5, 10] \times 10^{15}$ molecules cm^{-2} based on our analysis discussed below.

The distribution of OmF of all pixels over our domain from January 2013 to September 2014 is Gaussian except for its tails and 97 % of the OmF is in the interval of $[-5, 10] \times 10^{15}$ molecules cm^{-2}. However, over highly polluted areas both satellite observations and model results have larger errors resulting in higher OmF values. In addition, the lifetime of NO_2 is much longer in winter than in summer. Therefore, the NO_2 column concentration is higher than in summer, which may lead to large OmF values in winter time. We choose 15 high-polluted cities in China based on AQI and study the distribution of the OmF for the summer period (April to September 2013) and the winter period (October 2013 to March 2014) (Fig. 7). As expected, the distribution of OmF is wider in winter than in summer. In summer, 70 % of the OmF values are in the interval of $[-5, 10] \times 10^{15}$ molecules cm^{-2}, while in winter 50 % of the OmF values are within $[-5, 10] \times 10^{15}$ molecules cm^{-2}. We select an asymmetric interval because the assimilation is especially sensitive to very negative outliers in OmF caused by low observations (having small observational errors associated), as opposed to very positive outliers caused by high observations, which are associated with large observational errors. The observations with low error have more weight in the data assimilation process. To figure out the effect of a large OmF on NO_x emission estimates, we compare a free run of CHIMERE v2013 with the MEIC inventory with a run with the DECSO v3b assimilation. During the summertime, the difference in the seasonal average of the NO_2 column concentration between these two runs is 4.8×10^{15} molecules cm^{-2} in the Nanjing area (six grid cells). This column difference is caused by the NO_x emission difference of 9.2×10^{15} molecules cm^{-2} h^{-1}. From a simple back-of-the-envelope calculation we derive that a negative 5×10^{15} molecules cm^{-2} difference in NO_2 columns requires a 9.6×10^{15} molecules cm^{-2} h^{-1} emission change, which would mean that all NO_x emissions in Nanjing would

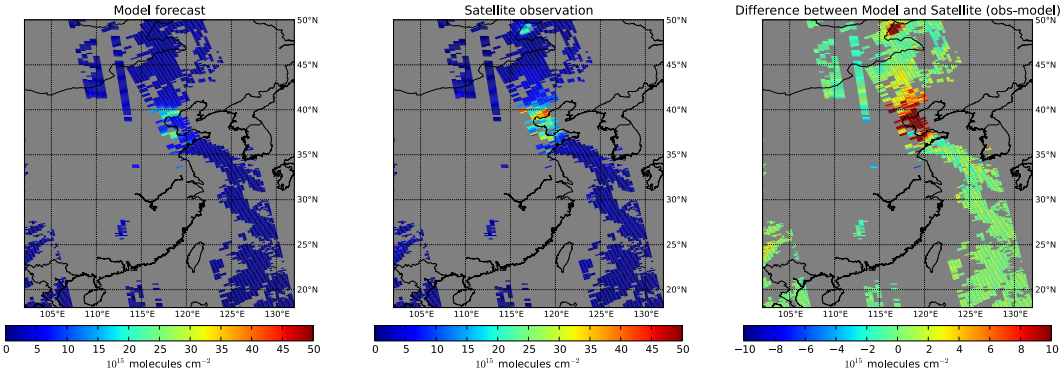

Figure 5. The comparison of the CHIMERE v2013 forecast (left) with OMI satellite observations (middle) on 6 May 2013. The right plot shows the difference between observations and forecast (OmF).

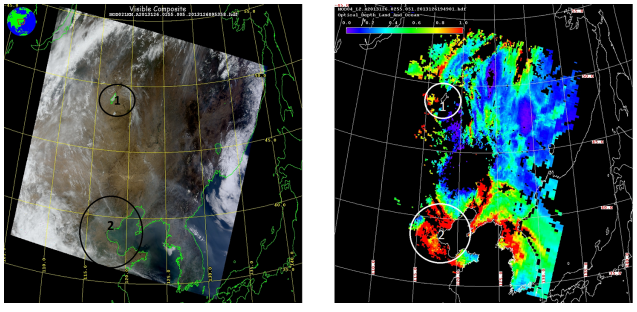

Figure 6. The RGB image (left) and Aerosol Optical Depth (right) from MODIS on 6 May 2013. Circle 1 and circle 2 represent the Hulunbuir sand land and the Bohai Bay respectively. (The figures are from https://ladsweb.nascom.nasa.gov/browse_images/granule_browser.html).

be removed in a single day. This change in emission is comparable to the total emissions of two large-sized coal-fired power plants. This shows that a change in OmF of 5×10^{15} molecules cm^{-2} is very unrealistic even in the most extreme cases. Therefore, this limit will be used as a criterion to filter outliers, which are in general caused by wrong NO_2 retrievals. To avoid the influence of the extreme OmF on emission estimates and still be able to monitor real emission changes, we filter out negative OmF values lower than 5×10^{15} molecules cm^{-2} and positive OmF values more than 10×10^{15} molecules cm^{-2} to be conservative. After applying the OmF filter criteria, we filter out 16 % of the extreme OmF in the polluted cities and less than 3 % in the whole domain. The large unrealistic jumps in emission disappear from the time series.

4 Emission analysis for the Nanjing Youth Olympic Games

First, we compare NO_2 monthly average concentrations in 2014 with previous years using in situ and satellite observations. For the in situ observations we select the monthly mean at 13:00 LT to be able to compare the results with the satellite observations whose overpass time is about 13:30 LT (see Fig. 8), which is also the average overpass time in Nanjing. Compared to the year 2013 the in situ measurements show no significant improvement in the surface NO_2 concentration at 13:00 LT for the period May to August 2014 when the government took air quality regulations for the YOG. However, we see a high variability in the monthly averaged data, indicating that the data are strongly affected by highly variable local sources (e.g. local traffic) and weather. We also calculate the monthly average using all measurements and we still see a high variability in the time series. Because of the high variability in the ground data and its low representativity for the whole city of Nanjing, we discarded this data set in our analysis.

Figure 1 shows the land-use over Jiangsu Province. The rectangle referred to as the Nanjing area covers the whole of Nanjing including all industrial areas along the Yangtze River. According to the MEIC sector distribution, the power plants in the selected area are dominating the NO_x emissions. To study the effects of the air quality regulations for the YOG on tropospheric NO_2 column concentrations, we compare the monthly averages of satellite observations over the Nanjing area for each year from 2005 to 2014 by regridding the observational data on the model grid over the area.

The satellite observations show that on average the NO_2 column concentrations are rather similar from year to year (Fig. 9). Although a small increasing trend from 2005 to 2011 is visible in the satellite data, it is negligible compared to the SD of the natural variability. It is clear that the NO_2 columns have a seasonal cycle that is lower in summer than in winter due to the seasonal change of the NO_2 lifetime (van der A et al., 2006). Note that the small decrease in columns in February might be caused by the reduced emissions during the Spring Festival (Q. Zhang et al., 2009). The monthly averages of NO_2 in situ observations shown by Wang et al. (2011) for Beijing, Shanghai and Guangzhou in 2005 were also re-

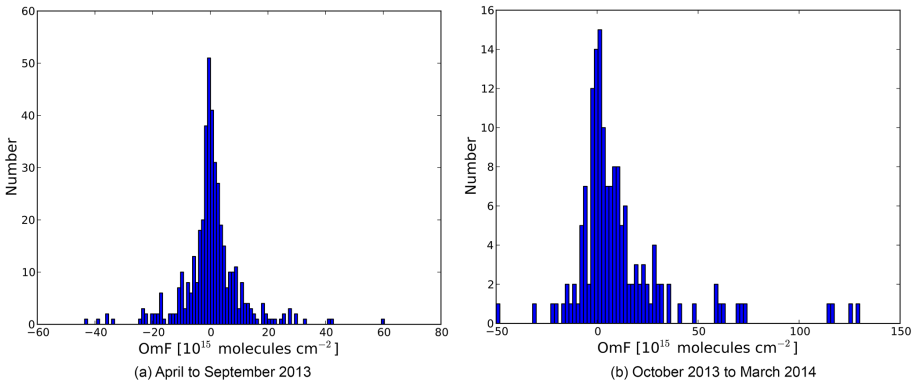

Figure 7. The distribution of the OmF values over 15 polluted cities in summer **(a)** and in winter **(b)**. The 15 polluted cities are Baoding, Beijing, Chengdu, Harbin, Hohhot, Guangzhou, Jinan, Shanghai, Shenyang, Shijiazhuang, Tianjin, Wuhan, Xi'an, Xingtai and Zhengzhou.

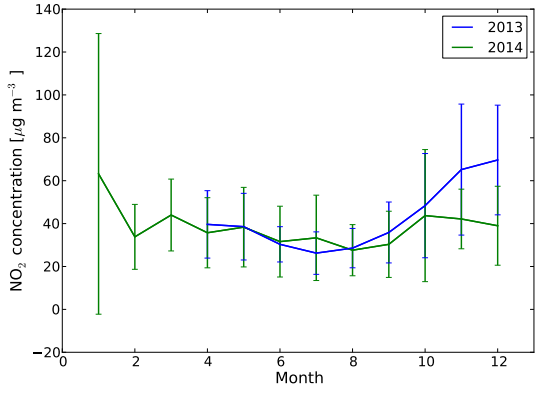

Figure 8. The monthly averaged in situ NO_2 concentration at 13:00 local time in Nanjing for 2013 and 2014. The bar is the standard deviation (natural variability) of the observations for each month (derived from the daily data on www.aqicn.org).

duced by around 10 % in February. We see that the NO_2 column during the YOG period (August 2014) is on average only 6.6×10^{15} molecules cm^{-2}, which is the lowest value among the last 10 years and more than 3 standard deviations from the mean. Possibly due to the effect of the continuous air quality regulations for the YOG and afterwards, the NO_2 columns of the following months are also lower than for previous years. The more permanent measures (traffic-related) resulting from the YOG affect a small fraction of the total emissions. In November, the local government took similar air quality regulations for the first National Memorial ceremony held on 13 December 2014. That might explain the lower NO_2 columns of the last 2 months of 2014 compared to those of 2013 and compared to the average of the last 8 years. However, it is still within the range of the standard deviation of NO_2 columns for the last 8 years. Differences from year to year can also be attributed to the meteorological conditions (Lin et al., 2011). Particularly in December 2013, NO_2 columns are very high. This episode is well known as a heavy smog period in Nanjing because stagnant air in the region accumulated anthropogenic pollution. Compared to the averaged NO_2 column in August from 2005 to 2012, the NO_2 column of August in 2014 is decreased by 32 % in Nanjing. However, this significant decrease can be caused by the rainy weather during that month. Thus, NO_x emission estimates are needed to show if the air quality regulations were really effective. The emission estimates use not only satellite observations in the location of the YOG but use all observations over China that are transported to and from Nanjing. Besides transport of air, the meteorological effect on the lifetime of NO_2 is taken into account.

To compare the NO_x emissions in Nanjing in 2014, especially during the YOG, with the same period of the year 2013, we run DECSO v3b with the OmF criterion as described in Sect. 3.2 from October 2012 to December 2014, where the first 3 months are used as a spin-up period. Figure 10 shows the monthly NO_x emissions in Nanjing for the year 2013 and 2014 estimated by this version of DECSO. For comparison the initial MEIC inventory is also plotted in the figure. The NO_x emissions have a different seasonal cycle compared to the NO_2 columns of satellite observations in Nanjing. The months with high emissions are June and July while the highest NO_2 columns of the satellite observations appear in January and December. According to the sector distribution in the MEIC inventory, the emissions of power plants and industrial activities are the main sources in Nanjing. At least 50 % of the total NO_x emissions are from power plants and 40 % are from the industrial activities. H. Zhang et al. (2009) showed that the seasonal cycle of the electricity consumption in Nanjing for the 7 years from 2000 to 2006 peaks in the summertime, because the electricity consumption and power load are highly correlated with temperature in summer. The value of electricity consumption in summer is at least two times higher than in winter every year and keeps increasing during those 7 years. The seasonality of electricity consumption is caused by the increasing usage of air conditioning in the hot season, while there is no

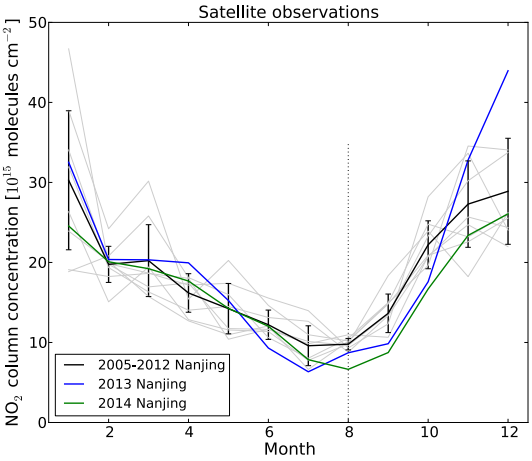

Figure 9. The monthly averages of OMI satellite observations of tropospheric NO_2 concentrations. The solid lines are the measurements over the Nanjing area. The grey lines are the monthly averages for each year from 2005 to 2012 to indicate the annual variability. The black lines show the average value for the years from 2005 to 2012. The bars are the standard deviations of monthly NO_2 observations from 2005 to 2012.

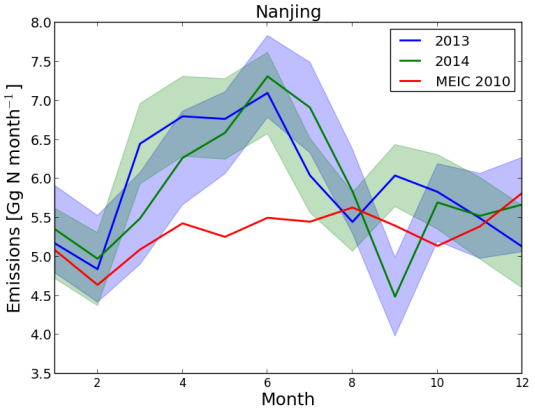

Figure 10. The monthly NO_x emission estimates by DECSO in Nanjing for 2013 (blue line) and 2014 (green line) and the monthly NO_x emission of the MEIC inventory of 2010 (red line). The shade areas show the error of the mean NO_x emission estimates from DECSO.

heating system used in winter time in Nanjing. The opposite cycles of column concentrations (Fig. 9) and emissions (Fig. 10) show that the high NO_2 concentrations in winter in Nanjing are mainly affected by the long lifetime of NO_x, while the seasonal cycle of NO_x emissions is reversed as a result of the increased electricity consumption in summertime. The difference with the seasonal cycle of MEIC might be attributed to the fact that our results are derived on city-level, while the seasonal cycle for bottom-up inventories are often derived on a national or provincial scale (e.g. Q. Zhang et al., 2009). The monthly average temperatures from June to September are above 20°. The monthly temperatures in 2014 did not deviate much from the climatological values.

We see a drop in NO_x emissions in February for both years calculated with DECSO, which is also visible in the MEIC inventory of 2010 (Fig. 10). This jump is consistent with the decrease of NO_2 columns of the satellite observations in February compared to the neighboring months. Compared to the neighboring months, the NO_x emission reduction in February is about 10 % in 2013 and 2014. This NO_x emission decrease was also noticed by Q. Zhang et al. (2009) in the INTEX-B inventory and likely to be caused by the reduced industrial activities during the Spring Festival. Lin and McElroy (2011) also showed that the Spring Festival causes a reduction of about 10 % on NO_x due to the decrease of thermal power generation based on the analysis of several satellite observations. Interestingly, we do not see an increase of NO_x emissions in the December 2013 smog period. This shows that the smog is caused by the meteorological conditions rather than increased emissions.

Figure 10 shows a large reduction of NO_x emissions in September 2014. The total NO_x emissions in September in Nanjing are 4.5 Gg N. Compared to the same time of the year 2013, the reduction is about 25 %. However, the emission reduction in this case seems to have a delay of 1 month. The shaded area in Fig. 10 represents the error on the derived emissions without taking into account the error introduced by the Kalman Filter time lag. Reductions in emissions at the end of August or the following months can appear with a time lag in the Kalman filter results (see e.g Brunner et al., 2012). This time lag is not fixed but depends on the amount, interval, accuracy and distance of the observations and it is therefore difficult to quantify. In our case, this is partly a consequence of the use of monthly means, while the regulations became active at the end of August. It is also a consequence of the lack of satellite observations due to the rainy (and therefore cloudy) weather in the second half of August 2014 when the YOG took place. For these kind of conditions, DECSO only detects the full extent of the emission reduction in September. We also see a NO_x emission reduction of 10 % in August 2013, compared to the neighboring months. One likely reason for this reduction is that the Asian Youth Games were held during that time. The local government also took measures to ensure good air quality for that event but they were not as strict as for the YOG in 2014. We conclude that the NO_x emission reduction detected by DECSO for the YOG period and afterwards was at least 25 %, showing that the air quality regulations taken by the local government were effective.

5 Discussion and conclusions

In this study the effect of the air quality regulations of the local government during the YOG in Nanjing in 2014 has been

quantified by analyzing observations on the ground and from the satellite. The focus in this study was on the reduced NO_2 concentrations and NO_x emissions. We compared NO_2 during the YOG period with previous years using the in situ and the OMI satellite observations. The in situ observations have a large variability, even after averaging on a monthly basis. This is probably caused by the variability of local sources and it indicates that these in situ observations are not representative for the larger area of Nanjing. The in situ data show no significant decrease during the YOG period. Since we have no error estimates of the in situ observations and very little information on the instrument and measurement techniques we discard the results of the in situ observations in our conclusions.

For the view from space we limited ourselves to retrievals of tropospheric NO_2 from OMI, taking advantage of the high spatial resolution of OMI observations compared to similar instruments. The monthly OMI satellite observations showed a 32 % decrease of the NO_2 column concentration during the YOG period in Nanjing compared to the average value for the last 10 years. However, the decrease of NO_2 columns observed by the satellite is not an objective measure to verify the impact of the air quality regulations taken by the local government, because changes in NO_2 columns can have more causes such as horizontal transport of NO_2 or increased wet deposition of the NO_2 reservoir gas NO_3 due to the rainy weather. Furthermore, due to cloudy conditions, the August average of 2014 is based on few observations. Therefore, it is important to analyze the emissions to show if the air quality regulations have really affected the NO_2 concentrations.

The results of our improved emission estimate algorithm DECSO show that NO_x emissions decreased by at least 25 % in September 2014, which shows that the air quality regulations were effective during the YOG period and that only a small part of the reduced NO_2 column concentrations were caused by the weather conditions. However, the reduction has a 1 month delay in our results. This is because satellite observations were scarce in the Nanjing area during the YOG (16 to 29 August), causing the DECSO algorithm to converge slower to the new emissions, which is typical for the Kalman filter approach used in DECSO. Although the strong point of Kalman Filter is its detailed error analysis, this time lag is not incorporated in its error formalism. In future research we intend to reduce this time lag by using a smoothing Kalman filter technique.

We were able to see the emission reduction of NO_x in the selected six grid cells representative for the Nanjing area. That means that DECSO is at least able to estimate NO_x emissions on a spatial resolution of about $50 \times 90\,km^2$. If we apply the same analysis on single grid cells the results are noisier because the footprint of the OMI covers on average a larger area than a single grid cell. To achieve emission estimates in a smaller area, either satellite observations with a higher spatial resolution are required or longer time periods should be considered.

The quality of our emission estimates is highly related to the quality of the model and the satellite observations. We improved the DECSO algorithm by using a new version of the CTM: CHIMERE v2013 instead of CHIMERE v2006. The comparison of OmF between two models showed that CHIMERE v2013 has a better performance in summertime. Good quality of satellite observations is also essential for emission estimates. The DOMINO retrieval algorithm does not properly account for the effects of high aerosol concentrations, which are common in China, on the retrieved NO_2 columns. In case of high aerosol concentrations, the difference between the model simulations and the retrievals is very large, which leads to wrong updates of NO_x emissions in DECSO. To improve the satellite observations we have set an OmF criterion to filter out erroneous observations and to avoid unrealistic NO_x emission updates. We set the limitation to the range -5 to 10×10^{15} molecules cm^{-2} for the OmF. With this filter criterion, the unrealistic updates of NO_x emissions are mostly prevented. We will further analyze the impact of high aerosol concentrations on the retrieved NO_2 columns in future research.

Furthermore, we observed an opposite seasonal cycle of NO_x emissions compared to the NO_2 columns observed by OMI satellite. The seasonal cycle of NO_x emissions is not the same for the whole China domain since the different climate in the north and the south of China leads to a different seasonality of energy consumption during the year. In Nanjing, as in most parts of southern China, people use air conditioning in summer and do not use heating systems in winter. This leads to a larger electricity production of power plants in summer resulting in higher NO_x emissions. Tu et al. (2007) studied the air pollutants in Nanjing and also found high NO_2 columns in winter but concluded that the high NO_2 columns were caused by high NO_x emissions in winter, while our emission estimates show the opposite. Wang et al. (2007) analyzed the seasonality of NO_x emissions based on GOME satellite observations for the regions north and south of the Yangtze River, defined as north and south China. Their results of south China showed the same seasonal cycle of NO_2 columns but a very weak seasonality of NO_x emissions and they also concluded that the NO_x lifetime mainly determines the NO_2 columns. Ran et al. (2009) explained high NO_x concentrations in winter are caused by slower chemical processes and shallow boundary layers contributing to accumulation of NO_x. The table in Wang et al. (2012) of annual and summer NO_x emissions from coal-fired power plants in 2005–2007 for different provinces in China showed that the NO_x emissions in Jiangsu Province in summer are higher than mean seasonal emissions.

In conclusion, we not only found a reversed seasonal cycle peaking in summertime in the emission estimates, but also indications for reduced emissions during the Spring Festival, the Asian Youth Games in 2013 and the YOG 2014. Based on our emission estimates the air quality regulation during the YOG 2014 and afterwards reduced the NO_x emissions

by at least 25 percent. This, together with favorable meteorological conditions, was responsible for a decrease of 32 % in NO_2 column concentrations observed from space. For the case of the YOG, our results can help the local government to identify the impact of their air quality regulations on reducing NO_x emissions.

The Supplement related to this article is available online at doi:10.5194/acp-15-9399-2015-supplement.

Acknowledgements. The research was part of the GlobEmission Project funded and supported by the European Space Agency. We acknowledge Tsinghua University for providing the MEIC inventory and the ESA GlobCover 2009 Project for the land use data set. The MODIS images used in this study were acquired as part of the NASA's Earth-Sun System Division and archived and distributed by the MODIS Adaptive Processing System (MODAPS). The OMI is part of the NASA Earth Observing System (EOS) Aura satellite payload. The OMI project is managed by the Netherlands Space Office (NSO) and the Royal Netherlands Meteorological Institute (KNMI).

Edited by: G. Frost

References

Acarreta, J. R., De Haan, J. F., and Stammes, P.: Cloud pressure retrieval using the O_2-O_2 absorption band at 477 nm, J. Geophys. Res., 109, D05204, doi:10.1029/2003JD003915, 2004.

Bessagnet, B., Hodzic, A., Vautard, R., Beekmann, M., Cheinet, S., Honoré, C., Liousse, C., and Rouil, L.: Aerosol modeling with CHIMERE – preliminary evaluation at the continental scale, Atmos. Environ., 38, 2803–2817, doi:10.1016/j.atmosenv.2004.02.034, 2004.

Blond, N., Boersma, K. F., Eskes, H. J., van der A, R. J., Van Roozendael, M., De Smedt, I., Bergametti, G., and Vautard, R.: Intercomparison of SCIAMACHY nitrogen dioxide observations, in situ measurements and air quality modeling results over Western Europe, J. Geophys. Res., 112, 1–20, doi:10.1029/2006JD007277, 2007.

Boersma, K. F., Eskes, H. J., Veefkind, J. P., Brinksma, E. J., van der A, R. J., Sneep, M., van den Oord, G. H. J., Levelt, P. F., Stammes, P., Gleason, J. F., and Bucsela, E. J.: Near-real time retrieval of tropospheric NO_2 from OMI, Atmos. Chem. Phys., 7, 2103–2118, doi:10.5194/acp-7-2103-2007, 2007.

Boersma, K. F., Eskes, H. J., Dirksen, R. J., van der A, R. J., Veefkind, J. P., Stammes, P., Huijnen, V., Kleipool, Q. L., Sneep, M., Claas, J., Leitão, J., Richter, A., Zhou, Y., and Brunner, D.: An improved tropospheric NO_2 column retrieval algorithm for the Ozone Monitoring Instrument, Atmos. Meas. Tech., 4, 1905–1928, doi:10.5194/amt-4-1905-2011, 2011.

Brunner, D., Henne, S., Keller, C. A., Reimann, S., Vollmer, M. K., O'Doherty, S., and Maione, M.: An extended Kalman-filter for regional scale inverse emission estimation, Atmos. Chem. Phys., 12, 3455–3478, doi:10.5194/acp-12-3455-2012, 2012.

Chan, C. and Yao, X.: Air pollution in mega cities in China, Atmos. Environ., 42, 1–42, doi:10.1016/j.atmosenv.2007.09.003, 2008.

Evensen, G.: The Ensemble Kalman Filter: theoretical formulation and practical implementation, Ocean Dynam., 53, 343–367, doi:10.1007/s10236-003-0036-9, 2003.

Hao, N., Valks, P., Loyola, D., Cheng, Y. F., and Zimmer, W.: Space-based measurements of air quality during the World Expo 2010 in Shanghai, Environ. Res. Lett., 6, 044004, doi:10.1088/1748-9326/6/4/044004, 2011.

He, K.: Multi-resolution Emission Inventory for China (MEIC): model framework and 1990–2010 anthropogenic emissions, in: International Global Atmospheric Chemistry Conference, 17–21 September, Beijing, China, available at: http://adsabs.harvard.edu/abs/2012AGUFM.A32B..05H (last access: 4 February 2015), 2012.

Irie, H.: Evaluation of long-term tropospheric NO_2 data obtained by GOME over East Asia in 1996–2002, Geophys. Res. Lett., 32, L11810, doi:10.1029/2005GL022770, 2005.

Irie, H., Boersma, K. F., Kanaya, Y., Takashima, H., Pan, X., and Wang, Z. F.: Quantitative bias estimates for tropospheric NO_2 columns retrieved from SCIAMACHY, OMI, and GOME-2 using a common standard for East Asia, Atmos. Meas. Tech., 5, 2403–2411, doi:10.5194/amt-5-2403-2012, 2012.

Itahashi, S., Uno, I., Irie, H., Kurokawa, J.-I., and Ohara, T.: Regional modeling of tropospheric NO_2 vertical column density over East Asia during the period 2000–2010: comparison with multisatellite observations, Atmos. Chem. Phys., 14, 3623–3635, doi:10.5194/acp-14-3623-2014, 2014.

Kroon, M., de Haan, J. F., Veefkind, J. P., Froidevaux, L., Wang, R., Kivi, R., and Hakkarainen, J. J.: Validation of operational ozone profiles from the Ozone Monitoring Instrument, J. Geophys. Res., 116, D18305, doi:10.1029/2010JD015100, 2011.

Kurokawa, J., Yumimoto, K., Uno, I., and Ohara, T.: Adjoint inverse modeling of NO_x emissions over eastern China using satellite observations of NO_2 vertical column densities, Atmos. Environ., 43, 1878–1887, doi:10.1016/j.atmosenv.2008.12.030, 2009.

Lamsal, L. N., Martin, R. V., Padmanabhan, A., van Donkelaar, A., Zhang, Q., Sioris, C. E., Chance, K., Kurosu, T. P., and Newchurch, M. J.: Application of satellite observations for timely updates to global anthropogenic NO_x emission inventories, Geophys. Res. Lett., 38, L05810, doi:10.1029/2010GL046476, 2011.

Leitão, J., Richter, A., Vrekoussis, M., Kokhanovsky, A., Zhang, Q. J., Beekmann, M., and Burrows, J. P.: On the improvement of NO_2 satellite retrievals – aerosol impact on the airmass factors, Atmos. Meas. Tech., 3, 475–493, doi:10.5194/amt-3-475-2010, 2010.

Levelt, P. F., van den Oord, G. H. J., Dobber, M. R., Malkki, A., Stammes, P., Lundell, J. O. V., and Saari, H.: The ozone monitoring instrument, IEEE T. Geosci. Remote Sens., 44, 1093–1101, doi:10.1109/TGRS.2006.872333, 2006.

Li, L., Chen, C. H., Fu, J. S., Huang, C., Streets, D. G., Huang, H. Y., Zhang, G. F., Wang, Y. J., Jang, C. J., Wang, H. L., Chen, Y. R., and Fu, J. M.: Air quality and emissions in the Yangtze River Delta, China, Atmos. Chem. Phys., 11, 1621–1639, doi:10.5194/acp-11-1621-2011, 2011.

Lin, J.-T. and McElroy, M. B.: Detection from space of a reduction in anthropogenic emissions of nitrogen oxides during the Chi-

nese economic downturn, Atmos. Chem. Phys., 11, 8171–8188, doi:10.5194/acp-11-8171-2011, 2011.

Lin, J.-T., Martin, R. V., Boersma, K. F., Sneep, M., Stammes, P., Spurr, R., Wang, P., Van Roozendael, M., Clémer, K., and Irie, H.: Retrieving tropospheric nitrogen dioxide from the Ozone Monitoring Instrument: effects of aerosols, surface reflectance anisotropy, and vertical profile of nitrogen dioxide, Atmos. Chem. Phys., 14, 1441–1461, doi:10.5194/acp-14-1441-2014, 2014.

Lin, W., Xu, X., Ge, B., and Liu, X.: Gaseous pollutants in Beijing urban area during the heating period 2007–2008: variability, sources, meteorological, and chemical impacts, Atmos. Chem. Phys., 11, 8157–8170, doi:10.5194/acp-11-8157-2011, 2011.

Liu, H., Wang, X., Zhang, J., He, K., Wu, Y., and Xu, J.: Emission controls and changes in air quality in Guangzhou during the Asian Games, Atmos. Environ., 76, 81–93, doi:10.1016/j.atmosenv.2012.08.004, 2013.

Martin, R. V., Jacob, D. J., Kurosu, T. P., Chance, K., Palmer, P. I., and Evans, M. J.: Global inventory of nitrogen oxide emissions constrained by space-based observations of NO_2 columns, J. Geophys. Res., 108, 4537, doi:10.1029/2003JD003453, 2003.

Menut, L., Bessagnet, B., Khvorostyanov, D., Beekmann, M., Blond, N., Colette, A., Coll, I., Curci, G., Foret, G., Hodzic, A., Mailler, S., Meleux, F., Monge, J.-L., Pison, I., Siour, G., Turquety, S., Valari, M., Vautard, R., and Vivanco, M. G.: CHIMERE 2013: a model for regional atmospheric composition modelling, Geosci. Model Dev., 6, 981–1028, doi:10.5194/gmd-6-981-2013, 2013.

Mijling, B. and van der A, R. J.: Using daily satellite observations to estimate emissions of short-lived air pollutants on a mesoscopic scale, J. Geophys. Res.-Atmos., 117, D17302, doi:10.1029/2012JD017817, 2012.

Mijling, B., van der A, R. J., Boersma, K. F., Van Roozendael, M., De Smedt, I., and Kelder, H. M.: Reductions of NO_2 detected from space during the 2008 Beijing Olympic Games, Geophys. Res. Lett., 36, L13801, doi:10.1029/2009GL038943, 2009.

Mijling, B., van der A, R. J., and Zhang, Q.: Regional nitrogen oxides emission trends in East Asia observed from space, Atmos. Chem. Phys., 13, 12003–12012, doi:10.5194/acp-13-12003-2013, 2013.

Miyazaki, K., Eskes, H. J., Sudo, K., Takigawa, M., van Weele, M., and Boersma, K. F.: Simultaneous assimilation of satellite NO_2, O_3, CO, and HNO_3 data for the analysis of tropospheric chemical composition and emissions, Atmos. Chem. Phys., 12, 9545–9579, doi:10.5194/acp-12-9545-2012, 2012.

Nanjing Statistical Bureau: Statistic Yearbook of Nanjing, China Statistic press, Beijing, 2013 (in Chinese).

Ran, L., Zhao, C., Geng, F., Tie, X., Tang, X., Peng, L., Zhou, G., Yu, Q., Xu, J., and Guenther, A.: Ozone photochemical production in urban Shanghai, China: Analysis based on ground level observations, J. Geophys. Res., 114, D15301, doi:10.1029/2008JD010752, 2009.

Richter, A., Burrows, J. P., Nüss, H., Granier, C., and Niemeier, U.: Increase in tropospheric nitrogen dioxide over China observed from space, Nature, 437, 129–32, doi:10.1038/nature04092, 2005.

Schmidt, H.: A comparison of simulated and observed ozone mixing ratios for the summer of 1998 in Western Europe, Atmos. Environ., 35, 6277–6297, doi:10.1016/S1352-2310(01)00451-4, 2001.

Shao, M., Tang, X., Zhang, Y., and Li, W.: City clusters in China: air and surface water pollution, Front. Ecol. Environ., 4, 353–361, doi:10.1890/1540-9295(2006)004[0353:CCICAA]2.0.CO;2, 2006.

Stammes, P., Sneep, M., de Haan, J. F., Veefkind, J. P., Wang, P., and Levelt, P. F.: Effective cloud fractions from the Ozone Monitoring Instrument: Theoretical framework and validation, J. Geophys. Res., 113, D16S38, doi:10.1029/2007JD008820, 2008.

Stavrakou, T., Müller, J.-F., Boersma, K. F., De Smedt, I., and van der A, R. J.: Assessing the distribution and growth rates of NO_x emission sources by inverting a 10-year record of NO_2 satellite columns, Geophys. Res. Lett., 35, L10801, doi:10.1029/2008GL033521, 2008.

Streets, D. G., Canty, T., Carmichael, G. R., de Foy, B., Dickerson, R. R., Duncan, B. N., Edwards, D. P., Haynes, J. A., Henze, D. K., Houyoux, M. R., Jacob, D. J., Krotkov, N. A., Lamsal, L. N., Liu, Y., Lu, Z., Martin, R. V., Pfister, G. G., Pinder, R. W., Salawitch, R. J., and Wecht, K. J.: Emissions estimation from satellite retrievals: A review of current capability, Atmos. Environ., 77, 1011–1042, doi:10.1016/j.atmosenv.2013.05.051, 2013.

Tu, J., Xia, Z.-G., Wang, H., and Li, W.: Temporal variations in surface ozone and its precursors and meteorological effects at an urban site in China, Atmos. Res., 85, 310–337, doi:10.1016/j.atmosres.2007.02.003, 2007.

Van der A, R. J., Peters, D. H. M. U., Eskes, H., Boersma, K. F., Van Roozendael, M., De Smedt, I., and Kelder, H. M.: Detection of the trend and seasonal variation in tropospheric NO_2 over China, J. Geophys. Res., 111, D12317, doi:10.1029/2005JD006594, 2006.

Wang, S., Zhao, M., Xing, J., Wu, Y., Zhou, Y., Lei, Y., He, K., Fu, L., and Hao, J.: Quantifying the air pollutants emission reduction during the 2008 olympic games in Beijing, Environ. Sci. Technol., 44, 2490–2496, 2010.

Wang, S., Xing, J., Chatani, S., Hao, J., Klimont, Z., Cofala, J., and Amann, M.: Verification of anthropogenic emissions of China by satellite and ground observations, Atmos. Environ., 45, 6347–6358, doi:10.1016/j.atmosenv.2011.08.054, 2011.

Wang, S. W., Zhang, Q., Streets, D. G., He, K. B., Martin, R. V., Lamsal, L. N., Chen, D., Lei, Y., and Lu, Z.: Growth in NO_x emissions from power plants in China: bottom-up estimates and satellite observations, Atmos. Chem. Phys., 12, 4429–4447, doi:10.5194/acp-12-4429-2012, 2012.

Wang, Y., McElroy, M. B., Martin, R. V., Streets, D. G., Zhang, Q., and Fu, T. M.: Seasonal variability of NO_x emissions over east China constrained by satellite observations: Implications for combustion and microbial sources, J. Geophys. Res.-Atmos., 112, 1–19, doi:10.1029/2006JD007538, 2007.

Wang, Y., Hao, J., McElroy, M. B., Munger, J. W., Ma, H., Chen, D., and Nielsen, C. P.: Ozone air quality during the 2008 Beijing Olympics: effectiveness of emission restrictions, Atmos. Chem. Phys., 9, 5237–5251, doi:10.5194/acp-9-5237-2009, 2009.

Witte, J. C., Schoeberl, M. R., Douglass, A. R., Gleason, J. F., Krotkov, N. A., Gille, J. C., Pickering, K. E., and Livesey, N.: Satellite observations of changes in air quality during the 2008 Beijing Olympics and Paralympics, Geophys. Res. Lett., 36, L17803, doi:10.1029/2009GL039236, 2009.

Wu, F. C., Xie, P. H., Li, A., Chan, K. L., Hartl, A., Wang, Y., Si, F. Q., Zeng, Y., Qin, M., Xu, J., Liu, J. G., Liu, W. Q., and Wenig, M.: Observations of $SO_2$2 by mobile DOAS in the Guangzhou eastern area during the Asian Games 2010, Atmos. Meas. Tech., 6, 2277–2292, doi:10.5194/amt-6-2277-2013, 2013.

Zhang, H., Sun, Z., Zhen, Y., Zhang, X., and Yu, B.: Impact of Temperature Change on Urban Electric Power Load in Nanjing, Transations Atmos. Sci., 32, 536–542, 2009.

Zhang, Q., Streets, D. G., He, K., Wang, Y., Richter, A., Burrows, J. P., Uno, I., Jang, C. J., Chen, D., Yao, Z., and Lei, Y.: NO_x emission trends for China, 1995–2004: The view from the ground and the view from space, J. Geophys. Res., 112, D22306, doi:10.1029/2007JD008684, 2007.

Zhang, Q., Streets, D. G., Carmichael, G. R., He, K. B., Huo, H., Kannari, A., Klimont, Z., Park, I. S., Reddy, S., Fu, J. S., Chen, D., Duan, L., Lei, Y., Wang, L. T., and Yao, Z. L.: Asian emissions in 2006 for the NASA INTEX-B mission, Atmos. Chem. Phys., 9, 5131–5153, doi:10.5194/acp-9-5131-2009, 2009.

Zhao, C. and Wang, Y.: Assimilated inversion of NOx emissions over east Asia using OMI NO_2 column measurements, Geophys. Res. Lett., 36, L06805, doi:10.1029/2008GL037123, 2009.